



# The role of cavitation in the toughening of elastomer nanocomposites reinforced with graphene nanoplatelets

Conor T. O'Brien<sup>a</sup>, Zheling Li<sup>b</sup>, Mufeng Liu<sup>a</sup>, J. Robert Innes<sup>a</sup>, Suhao Li<sup>a</sup>,  
Dimitrios G. Papageorgiou<sup>c</sup>, Malte Storm<sup>d</sup>, Timothy L. Burnett<sup>e,\*</sup>, Robert J. Young<sup>a,\*</sup>

<sup>a</sup> National Graphene Institute and Department of Materials, University of Manchester, Manchester M13 9PL, UK

<sup>b</sup> College of Aerospace Engineering, Chongqing University, Chongqing 400044, China

<sup>c</sup> School of Engineering and Materials Science, Queen Mary University of London, London E1 4NS, UK

<sup>d</sup> Diamond Light Source, Harwell Science & Innovation Campus, Didcot, Oxfordshire OX11 0DE, UK

<sup>e</sup> Henry Royce Institute and Department of Materials, University of Manchester, Manchester M13 9PL, UK

## ARTICLE INFO

### Keywords:

Nanocomposites  
Graphene  
Failure  
X-ray CT analysis

## ABSTRACT

The toughening of different types of elastomers through the incorporation of graphene nanoplatelets (GNPs) has been investigated. Both the tear strength and tearing energy are increased significantly through a combination of mechanisms such as debonding, pull-out and cavitation. The processes that occur ahead of a tear/crack tip in natural rubber filled with GNPs have been monitored in situ using synchrotron-based nanoscale X-ray computed tomography. The GNP particles are found to debond and form voids that grow under stress leading to considerable energy absorption. The mechanisms of cavitation and void growth are analysed theoretically and it is shown that voids need to be larger than  $\sim 1 \mu\text{m}$  in size to grow in the triaxial tensile stress field ahead of the tear/crack tip. The high level of cavitation and void growth found for the elastomers filled with micron-sized GNP particles is suggested to be the reason why these nanocomposites have a high tear resistance.

## 1. Introduction

Elastomers are used widely in engineering applications such as automotive and aerospace because of their excellent and unique mechanical properties. Their resistance to failure through tearing is a crucial consideration for the application of different elastomers. Historically the tear resistance of elastomers has been improved through the addition of fillers such as a carbon black. Azura and Leow [1] investigated the effect of carbon black (CB) loading upon the tear strength of natural rubber (NR) and found that there was an approximately linear increase in tear strength with CB loading. They also studied the effect of the type of carbon black upon the tear resistance and found that for a given CB loading the highest tear strength was found for the smallest type of carbon black (N220). Li and co-workers [2] undertook a similar study of the properties of natural rubber with different contents of carbon black and found a similar linear increase in tear strength with CB loading. A study upon styrene-butadiene rubber (SBR) by Berki and co-workers [3] again showed an approximately linear increase in tear strength upon the addition of two different types of carbon black particles.

There is considerable interest in understanding the mechanisms responsible for the increase in the tear strength of different rubbers upon the addition of fillers such as carbon black. It is rather difficult to do so as CB is a nano-sized filler and post-mortem analysis is not always reliable in these soft nanocomposites. A technique that has proved to be particularly useful in the analysis of processes that take place during the deformation of filled rubber is small-angle X-ray scattering (SAXS), since it is particularly sensitive to detecting the formation of nano-size cavities and voids. In 1990, Figuiera [4] reported a study of the deformation of CB-filled natural rubber using synchrotron SAXS and was not able to find any voiding during deformation up to 100 % strain. Zhang *et al.* [5] used a highly-collimated micro-X-ray beam at the European Synchrotron Radiation Facility (ESRF) to identify nano-cavitation near the crack tip in SBR filled with commercial CB materials under stress from the increase in the intensity of the SAXS in the vicinity of the crack. A similar study by Euchler *et al.* [6] upon SBR found cavitation at the crack tip in the rubber under stress in the absence of filler but found less evidence for cavitation in the CB filled specimens. Xiang *et al.* [7] undertook a study of the processes taking place at the crack tip in CB-filled NR under stress using a combination of synchrotron-based small- and wide-angle X-ray

\* Corresponding authors.

E-mail addresses: [timothy.burnett@manchester.ac.uk](mailto:timothy.burnett@manchester.ac.uk) (T.L. Burnett), [robert.young@manchester.ac.uk](mailto:robert.young@manchester.ac.uk) (R.J. Young).

<https://doi.org/10.1016/j.compositesa.2024.108269>

Received 16 November 2023; Received in revised form 22 April 2024; Accepted 12 May 2024

Available online 13 May 2024

1359-835X/© 2024 The Authors. Published by Elsevier Ltd. This is an open access article under the CC BY license (<http://creativecommons.org/licenses/by/4.0/>).

scattering that enabled them to follow the competition between strain-induced crystallisation and cavitation. They showed that the addition of CB enhances strain-induced crystallisation but they did not observe any cavitation. They compared their findings with those of Euchler *et al.* [6] and concluded that the presence of CB may actually prevent cavity formation in rubber. This conclusion confirms the original finding of Figuera [4] that voiding is not a major mechanism involved in the deformation of CB-filled elastomers. Another complication is that the carbon black is often poorly dispersed in elastomers, mainly due to the inherent hydrophobic nature of both materials, and the CB particles can form large agglomerates. Kallungal *et al.* [8] investigated crack propagation in situ in ethylene propylene diene monomer (EPDM) elastomer containing large CB agglomerates with micron dimensions, using X-ray computed tomography (CT) [9]. They found that the agglomerates can undergo either fracture or arrest and deviate a crack during propagation but did not report any observations of significant cavitation or void growth.

It is well-accepted that graphene-based fillers can improve the multifunctional properties of rubbers as the result of their excellent intrinsic properties and high aspect ratios [10–14]. A detailed study has been undertaken upon the deformation and tearing of a fluoroelastomer (FKM) reinforced with graphene nanoplatelets (GNPs) by Liu and co-workers [15]. They evaluated the fracture energy for tearing using the pure shear test and it was shown that the tearing energy increased linearly with the volume fraction of the GNPs. They found that at a given GNP loading, the tearing resistance was 3 times higher than that of the unfilled FKM, suggesting significant toughening upon the addition of the GNPs. They undertook a theoretical analysis of the micromechanics of tearing by considering debonding and pull-out of the nanoplatelets as the possible toughening mechanisms. They determined quantitatively that the main toughening mechanism was through debonding of the interface rather than pull-out. The fracture energy for interfacial debonding was estimated to be 1 kJ/m<sup>2</sup>, which is significantly higher than that for conventional fibre/epoxy composites [16]. They found by using post-mortem scanning electron microscopy that cavities formed at the end of the flake during deformation, and suggested that cavitation might be an additional factor contributing to this remarkably high fracture energy of tearing.

In this present study we have investigated the effect of the addition of two different types of filler, CB and GNPs, upon the tear strength of three different elastomers: natural rubber (NR), a fluoroelastomer (FKM) and a nitrile butadiene rubber (NBR). In particular we have compared and contrasted the ability of fillers such as CB and GNPs to increase the tear resistance of FKM and NBR for a given loading. We have also examined tear propagation in an NR/GNP nanocomposite and employed nanoscale X-ray CT to follow cavitation in situ at the crack tip. The behaviour has been modelled in terms of the mechanics of void growth in elastomeric materials.

## 2. Materials and methods

### 2.1. Natural rubber nanocomposites

The natural rubber (NR) was provided by Astlett Rubber Inc., Oakville, Ontario, Canada and was used as received. The grade of rubber used was SMR CV60, which denotes Standard Malaysian Rubber with a Mooney-Viscosity ML (1 + 4, 100 °C) of 60. The graphene nanoplatelets (GNPs) were provided by XG Sciences, Lansing, Michigan, USA and used as received. The GNPs used were Grade-M particles with a lateral dimension of 15 µm (referred to as M15) with a nominal thickness of 6–8 nm (approximately 20 graphene layers, specific surface area ~ 100 m<sup>2</sup>/g) quoted by the manufacturer. Other additives used in the rubber processing, namely zinc oxide, stearic acid, CBS accelerator and sulphur, were of analytical grade and used as received. The formulations of the samples produced are listed in Table S1 in the Supplementary Information. Details of the processing of the NR/GNP nanocomposites into

sheets are given elsewhere [10]. Briefly, the rubber mastication was conducted using a Bridge two-roll mill. The additives and GNPs (Table S1) were added to the rubber in the mill when it became warm and sticky and mixing took place for 10 min during which time the rubber sheets were folded to achieve a good dispersion of the fillers. The compounds were then cut into pieces and moulded into ~ 2.5 mm thick sheets using a hot press. Vulcanisation took place by heating the sheets at 160 °C for 10 min in the press.

### 2.2. FKM rubber nanocomposites

The fluoroelastomer (FKM), Tecnoflon PFR 94 (Solvay Ltd.) was used as received. The graphene nanoplatelets (GNPs), received from Avanzare Ltd., coded as AVA-0240, with a specific surface area (BET) of 37 ± 12 m<sup>2</sup>/g [17], were mixed with the FKM. The other additives employed in rubber processing for more effective mixing and curing, peroxide (Luperox® 101XL45, Arkema Co. Ltd.) and triallyl isocyanurate (TAIC 50 Co-activator, Wilfrid Smith, Ltd.) were analytical grades and used as received. The formulations of the samples produced are listed in Table S2 in the Supplementary Information along with details of processing of the FKM/GNP nanocomposites into ~ 2.5 mm thick sheets.

### 2.3. Nitrile butadiene rubber (NBR) nanocomposites

The nitrile butadiene rubber (Nipol 1052 J with an acrylonitrile content of 33.5 %) was supplied by Clwyd Compounding. The n-cyclohexyl-2-benzothiazole sulphenamide (CBS) was also supplied by Clwyd Compounding. Sulphur, zinc oxide, tetramethylthiuram disulphide (TMTD), and stearic acid (SA) were purchased from Sigma-Aldrich and used as received. The formulations of the samples upon the addition of M15 GNPs produced are listed in Table S3 in the Supplementary Information along with details of the processing of the NBR/GNP nanocomposites into ~ 2.5 mm thick sheets.

### 2.4. Tear testing

#### 2.4.1. 90° tear test

Tear testing was performed upon the elastomer nanocomposites according to ASTM D624-C with a 90° notched sample for a consistent tear initiation site (Fig. 1(a)). The specimens were produced using a die and stamped out from the bulk nanocomposite sheets. The tear test specimen is extended as in a tensile test. However, due to the non-symmetrical shape of the sample, catastrophic failure occurs localised at the initiation site, controlled by the 90° notch. Force-extension curves were obtained from the angle-type test specimens, using an Instron 4301 machine under a cross-head speed of 500 mm min<sup>-1</sup>. At least five specimens of each sample type were tested and the average taken from a minimum of three specimens. The tear strength  $T_s$  is determined using the following equation

$$T_s = F/d \quad (1)$$

where  $F$  is the maximum force and  $d$  is the thickness of the test piece.

#### 2.4.2. Trouser tear test

The trouser tear test (ASTM D624-T) was also employed in order to follow crack propagation and determine the tearing resistance of the NR nanocomposites. In this case the sample was cut into a 50 mm × 20 mm rectangular sheet with a 20 mm notch introduced using a fresh razor blade. The notch was cut by successive passes of the blade to ensure a smooth cut.

The jaws of the mechanical testing machine were extended at a constant rate of extension of 500 mm min<sup>-1</sup> with the tear propagating along long axis of the specimen. The ASTM trouser tear strength for this specimen is again given by Equation (1), with  $F$  in this case being the median force during tear propagation.

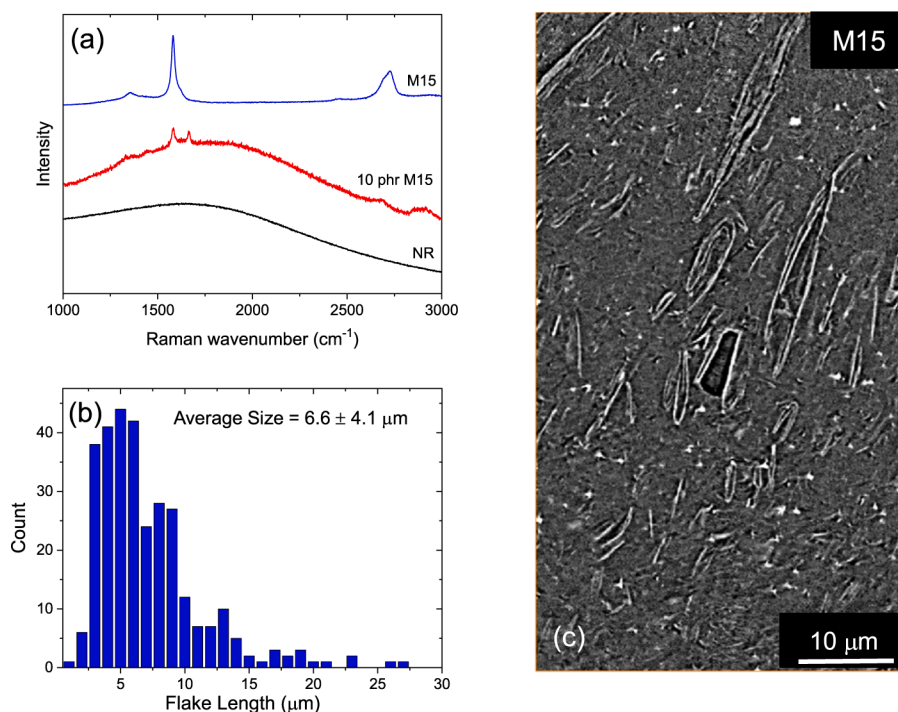


**Fig. 1.** (a) Raman spectra of the NR matrix, M15 GNPs and nanocomposite (NR/GNP – 10 phr). (b) Histogram of the distribution of measured lengths of the M15 GNPs determined using SEM. (c) Nano CT scan of the NR/GNP nanocomposite (The white dots are the ZnO additives (Table S1)).

## 2.5. Scanning electron microscopy (SEM)

Scanning Electron Microscopy was used in order to both determine the size of the GNPs and gain an insight into the fracture surfaces of the NR/GNP nanocomposites after mechanical testing. The GNP particles were sprinkled on aluminium stubs and their size distribution determined using a high resolution Philips XL 30 FEG SEM operated at 10 kV. Due to the insulating nature of NR, it was imperative to coat the samples in a conductive material in order to allow clear images to be obtained with no charging. This was carried out by applying a thin layer of platinum-gold alloy using a Quorum Q-Series sputter coater. The specimens were clamped to an SEM sample stub that allowed the fracture surface to be held perpendicular to the electron beam. A TESCAN Mira SEM was used to capture these images via the detection of secondary electrons. A beam voltage of 5 keV was employed, with an approximate working distance of 8 mm.

## 2.6. Raman spectroscopy

Characterisation of the NR nanocomposite materials was undertaken using a Renishaw 2000 Raman spectrometer with a 633 nm laser and an optical microscope with a  $\times 50$  objective lens that gave a spot size of the order of 2  $\mu\text{m}$ . Raman spectra were obtained both from low temperature fracture surfaces of the NR, NR nanocomposites (10 phr) and clusters of GNP particles on glass slides.

## 2.7. X-ray computed tomography (XCT)

A Zeiss Xradia Ultra 810 instrument was employed to obtain nanoscale X-ray CT data from undeformed specimens. Projections of the sample (801) were obtained using Zernike phase contrast in the ‘large field of view’ mode using a 30 s exposure time giving a 128 nm pixel size and field of view of 65  $\mu\text{m}$ .

X-ray CT images during deformation were obtained using the TXM (transmission X-ray microscope) setup at the I13–2 beamline at Diamond Light Source (DLS), Harwell, UK as shown in Figure S1

(Supplementary Information). This facility was used due to the increased beam flux compared to a laboratory-based set up, allowing for rapid image acquisition. A field of view (FOV) of either 65 or 88  $\mu\text{m}$  was used for the scans. Phase contrast mode was employed at an energy of 12 keV to allow clear visualisation of the different phases within the composite, as traditional attenuation contrast mode would not provide good contrast of the predominantly carbon-based components of GNPs and rubber. Two different modes of testing were carried out, namely static and dynamic tests. All data gathered were reconstructed using the Savu software [18] at the DLS and visualised using a range of software packages. In particular FIJI was used to examine individual cross-sectional slices of the samples, while AVIZO allowed for three-dimensional visualisation and analysis.

### 2.7.1. Dynamic imaging

Strips were cut from 100  $\mu\text{m}$  thick sheets of 10 phr GNP-rubber composite with a width of approximately 2 mm. These strips had a notch added horizontally across the 2 mm wide surface with a fresh razor blade to a depth of approximately 40–50  $\mu\text{m}$ . The strips were mounted into a Deben 2 kN rig and extended to a strain of up to 40 % until visible widening of the notch was seen. The strain was backed off, and then two pins were superglued to the sample, parallel to the notch and separated by approximately 5–6 mm with the notch centred between them. The sample was removed from the rig, and the strip of rubber trimmed with the ends wrapped around the pin and secured with superglue. A notched tube of Kapton (polyimide film - an X-ray transparent material) was used to hold the sample under a fixed strain of approximately 20–30 %, to monitor tear propagation as shown in Figure S2 (Supplementary Information).

The specimen was mounted on the rotation stage as shown in Figure S1 (Supplementary Information), and a series of time lapse radiographs were taken looking along the axis of the notch, i.e., parallel to the pins. Care was taken to track the crack tip, and to keep it within the field of view. A radiograph was captured every 10 s, with the large field of view (88  $\mu\text{m}$ ) selected giving a pixel size of  $\sim 80$  nm. It was possible to put the sequence of these scans together, giving a time-lapse video of

tear propagation in the specimen.

### 2.7.2. Static imaging

Static imaging refers to the fact that the crack does not propagate while the image is recorded. In fact, in this regime, the stage is rotated as described above. Fig. S3 (a) (Supplementary Information) shows the general set up of the experiment. A piece of rubber composite with a cross section of  $100 \times 100 \mu\text{m}^2$  was cut using a scalpel and attached to a pin with superglue, such that the rubber was positioned with a minimal amount standing proud of the pin. This was done to minimise lateral movement of the rubber with respect to the axis of rotation. The entire acquisition took approximately 30 min before reconstruction was carried out using Savu software. A field of view of  $65 \mu\text{m}$  was used, giving a resolution of approximately 60 nm. A series of scans were taken as a function of depth below the fracture surface, as depicted in Fig. S3 (b).

## 3. Results and discussion

### 3.1. Microstructural Characterisation

Raman spectroscopy was employed to characterise the GNPs, NR and NR/GNP nanocomposites as shown in Fig. 1(a). The GNPs show a spectrum typical of  $\text{sp}^2$  carbon materials with well-defined D, G and 2D bands [19]. On the other hand the NR spectrum shows only a broad fluorescent background. The NR/GNP nanocomposites show Raman bands from the GNPs superimposed on the fluorescent background of the NR matrix, typical of a nanocomposite containing a dispersion of nanofiller particles. Fig. 1(b) shows the distribution of GNP particle size measured using SEM. It can be seen that the majority of the particles have lengths in the size range 1–10  $\mu\text{m}$  with a median value of around 6  $\mu\text{m}$ . A nanoscale X-ray CT image of the NR/GNP nanocomposite before deformation is shown in Fig. 1(c). It can be seen that GNP nanoparticles are well distributed in the NR matrix with some preferential alignment. Moreover the CT scan shows that the GNPs tend to be curved, bent into loops and sometimes in clusters. Overall their sizes are consistent with

those reported in Fig. 1(b).

### 3.2. 90° tear tests

The dependence of the tear strength of the three different elastomers upon the volume fractions,  $V_f$  of GNPs or CB fillers is shown in Fig. 2(b-d). A comparison between the variation of the tear strength of NR, FKM and NBR upon the volume fractions of GNPs is shown in Fig. 2(b). The volume fractions were determined from the nominal compositions in phr (parts per 100 parts of rubber - see Supplementary Information) - and densities of the different elastomers and fillers. The actual loadings were also checked using thermogravimetric analysis (TGA). It can be seen that there is an approximately linear dependence of the tear strength upon  $V_f$  for all three types of nanocomposites. In addition it can be seen that the NR/GNP material has a higher tear strength than the other two filled materials. The tear strength of the unfilled NR is roughly twice that of the other two elastomers partly as the result of strain-induced crystallisation [7]. Moreover, the slopes of the lines on the plot for the different systems are roughly parallel to each other, implying that a similar mechanism is responsible for the additional increase in tear strength for the different elastomers upon the addition of the GNPs. A comparison has also been made of the effect of adding GNPs compared with CB to the FKM and NBR elastomers in Fig. 2(c-d). In both cases it can be seen that the addition of GNPs lead to a significantly higher tear strength for the nanocomposites than for the same loading of CB.

### 3.3. Trouser tear tests

The 90° tear test is widely employed to follow the tearing behaviour of elastomers. It involves both the initiation and propagation of a tear in the material and failure occurs in an unstable manner. In order to undertake an analysis of the mechanism of tearing using X-ray CT in the synchrotron, it was desirable to be in a regime whereby tearing occurs in a stable manner. Because of this the ASTM 634-T trouser tear test was also employed to characterise tearing in the NR/GNP material. There

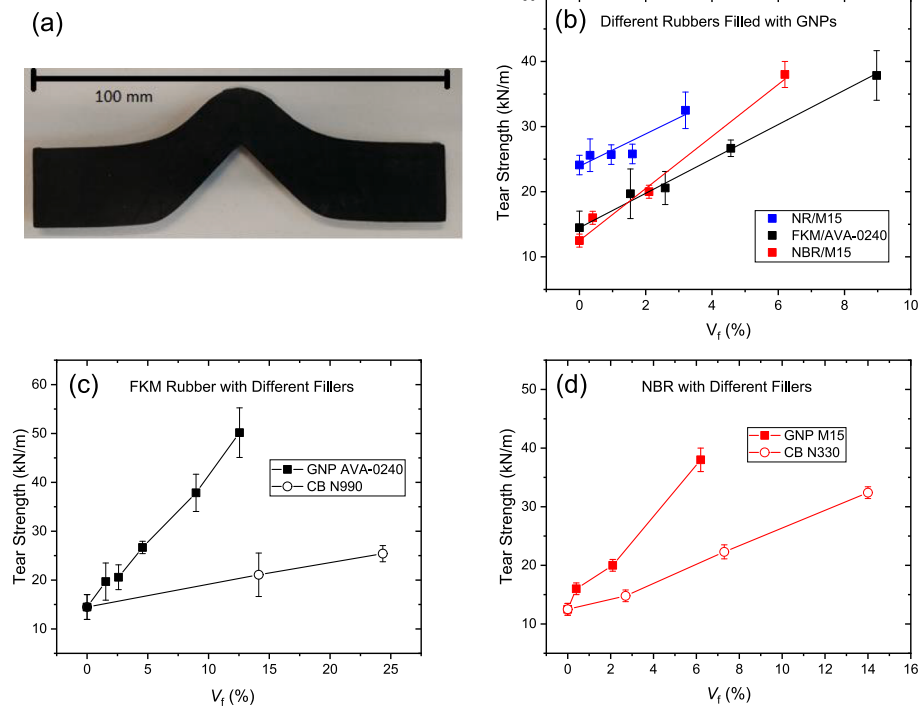


**Fig. 2.** Tear testing of the filled elastomers: (a) An ASTM D624-C standard 90° test specimen stamped from a moulded NR/GNP sheet. (b) The dependence of the tear strength for the three different elastomers as a function of GNP loading. (c) Comparison between the tear strength of the FKM rubber loaded with GNPs or CB. (d) Comparison between the tear strength of the NBR loaded with GNPs or CB.

has been a number of earlier studies upon the tearing of rubber materials using the trouser test. Sakulkaew, Thomas and Busfield [20] pointed out that cracks can grow in a number of different ways in this test, either by continuous tearing or discontinuous knotty or stick-slip tearing. The X-ray CT approach works well under conditions of steady tearing but is much more difficult to interpret if the rubber shows discontinuous crack growth. Fig. 3(a) shows that the pure rubber (0 phr) undergoes discontinuous knotty tearing whereas the tearing behaviour for rubber above 5 phr of GNPs is steady and continuous with a lower tear strength.

Sakulkaew *et al.* [20] undertook a detailed investigation into the factors that affect crack propagation behaviour in both natural rubber (NR) and styrene butadiene rubber (SBR), including cross-link density, tearing rate and the addition of carbon black. They showed that NR is particularly prone to discontinuous tearing as the result of crystallisation taking place at the crack tip under stress. They also found that changing the rate of testing by many orders of magnitude or the addition of 50 phr of carbon black to the NR did not strongly affect its behaviour. In our study we have shown that the addition of above around only 5 phr of GNPs has a major effect on the process of crack propagation in the NR, changing it from discontinuous to continuous. Because of this, NR with 10 phr of GNPs that undergoes continuous crack propagation was used for the monitoring of crack propagation using X-ray CT.

### 3.4. Tearing mechanisms

The fracture surfaces of the NR/GNP nanocomposites specimens were examined using SEM. Fig. 4(a) shows SEM images of opposing fracture surfaces with protruding GNPs and voids clearly visible. It can be seen that these surfaces can be pieced back together, like a “lock and key”, giving support to the well understood method of failure referred to as “pull out” [15,16]. A planar rubber surface is also seen, indicating that the crack propagates across the material in a way similar to that seen in brittle materials, even though large elastic deformations and retraction are involved.

Fig. 4(b) is a higher magnification image of the fracture surface and in particular a large void can be seen following the failure of the nanocomposite. The internal surface of the void is rough, seemingly indicating that the GNP that was previously in the void was not removed in one smooth action. The energy associated with the friction of sliding out a GNP from the matrix is often discussed during the analysis of tearing mechanisms [15]. It can also be seen that the remaining flakes are surrounded by voiding, which is often taken to indicate a poor interface between the matrix and the filler.

### 3.5. Nanoscale X-ray computed tomography

Individual components of the nanocomposites can be identified in a number of ways using X-ray CT. Voids and GNPs can be distinguished

from the bulk NR through their differences and changes in intensity, while the GNPs also exhibit sharp and angular edges. Due to the phase contrast imaging the contrast is related to the refractive index and not the electron density. Whilst phase contrast clearly highlights the GNP's edges in these images are also associated with ‘fringes’ meaning that a single phase is not represented by a single greyscale value. In order to obtain a representative volume of GNPs within the field of view of images and to ensure crack propagation by steady tearing, specimens with a loading of 10 phr of GNPs in NR were used throughout the X-ray CT analysis.

#### 3.5.1. Crack tip propagation

The tip of the tear was tracked as it propagated across the specimen suspended within the Kapton tube. This was done by moving the stage and taking successive radiographs. These images were combined into a time-lapse video from which still frames were taken to analyse the mechanism of tearing in the NR nanocomposite. A video of the process is available in the [Supplementary Information](#).

Fig. 5 shows a radiograph of the tear tip as it propagates across the sample. Also shown in the inset of the figure, is a schematic showing the orientation of the global sample, as well as the location of the field of view shown. It can be seen that the tip is blunt and rounded when the specimen is under stress whereas when the fracture surfaces were observed post-mortem they were found to be relatively smooth (Fig. 4). This shows that although the material undergoes high-strain deformation during tearing, it recovers elastically producing smooth fracture surfaces – a characteristic feature of crack propagation in rubber-elastic materials.

#### 3.5.2. Void formation

The onset of void formation, and their location relative to the crack tip, was also investigated. Fig. 6 shows two successive radiographs that show the tear tip highlighted in yellow on the left edge of the field of view. A region of nanocomposite is shown within a yellow box ahead of the crack within the bulk rubber material. It can be seen that a void forms around the GNP filler particle and that the GNP remains within the void.

The prevalence of voids beneath the fracture surface can also be investigated by analysing the cross section of the reconstructed volume of the fracture surface and the material beneath the surface in post-mortem tomography scans. The fracture surface and a volume that is located 600  $\mu\text{m}$  beneath the surface is shown in Fig. 6. Due to the fact that the images were captured using Zernike phase contrast [21], the bright white flares on the image can be attributed to the dramatic change in refractive index of the neighbouring components (GNPs and voids) in the nanocomposite. This is also seen at the surface, as the beam passes between the various components of the material and the surrounding air. It is also of particular use to help identify voids in the

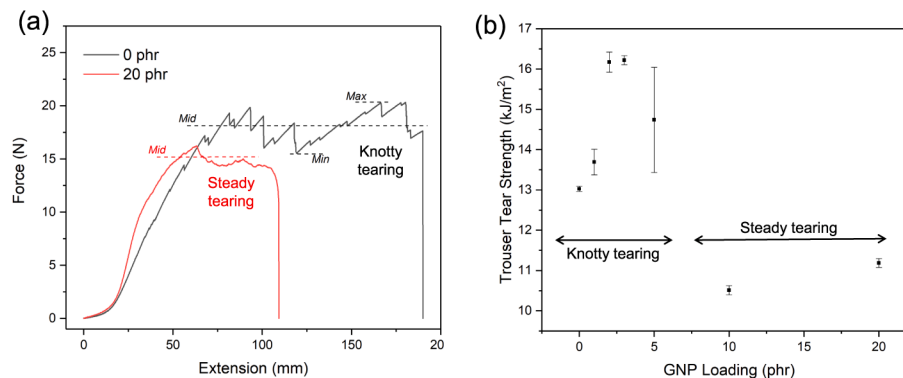
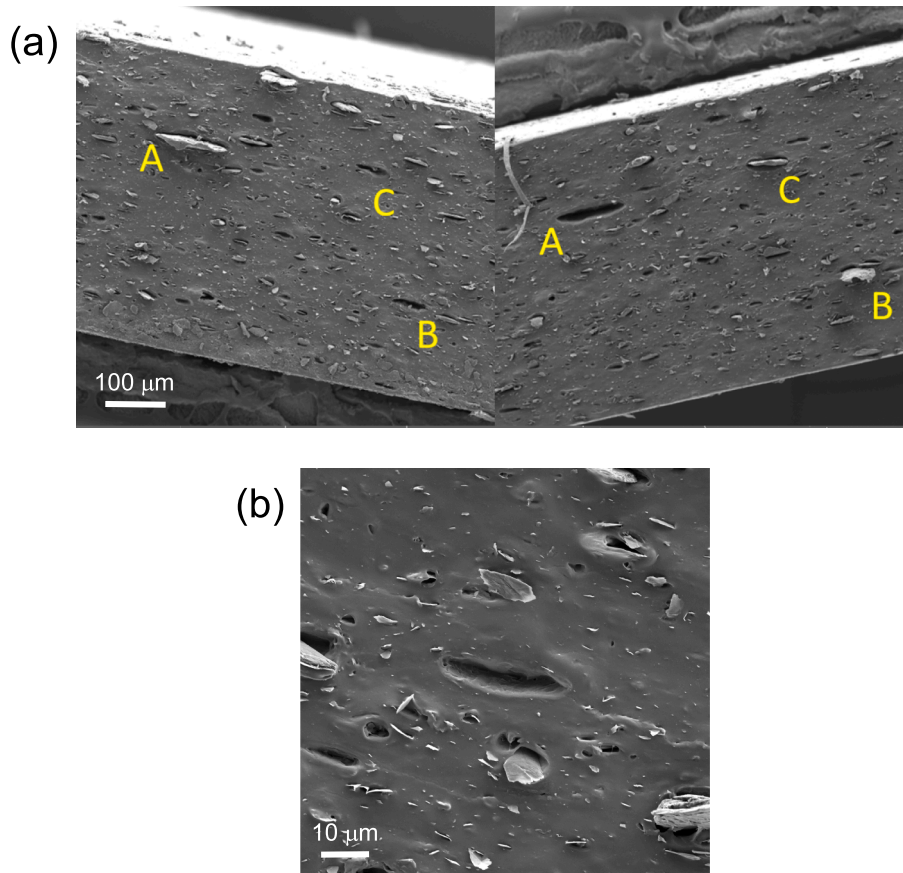
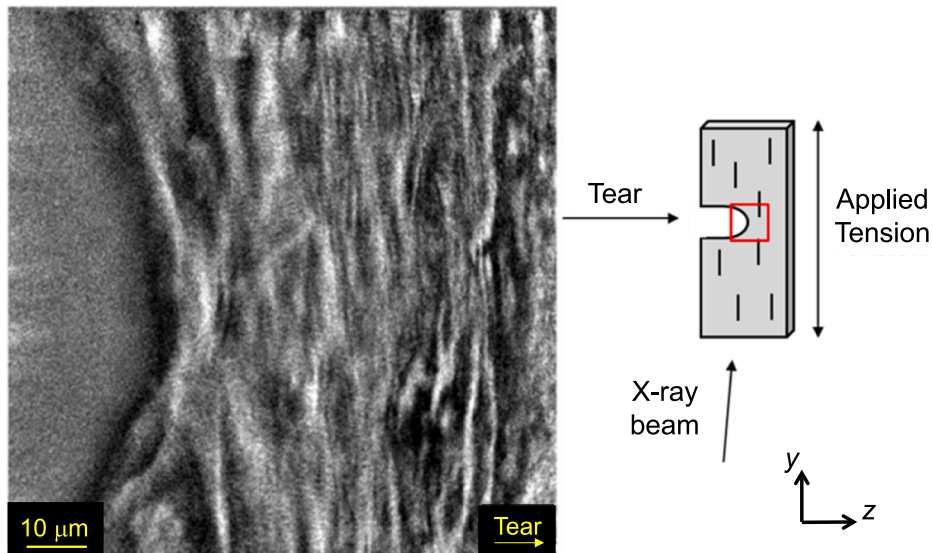


Fig. 3. (a) Representative force-extension curves for low (0 phr) and high (20 phr) NR/GNP nanocomposite specimens. The maximum, midpoint and minimum values at which tearing occurred are marked. (b) The trouser tear strength, calculated from midpoint force, is plotted as a function of GNP loading (phr).



**Fig. 4.** (a) Opposing fracture surfaces of a NR/GNP nanocomposite. Paired voids and GNPs are labelled A, B and C respectively. (b) A large void on the fracture surface of the nanocomposite. Voiding is seen surrounding the protruding GNP flakes.



**Fig. 5.** Radiograph showing the tip of a crack propagating across the sample (NR/GNP – 10 phr). A schematic is shown to illustrate the location of the crack tip. The vertical lines in the schematic portray the edges of the GNPs. The specimen coordinate system axes are given. (This is a still image from the time-lapse video in the Supplementary Information (S3)).

region beneath the fracture surface.

In the first image of Fig. 7 (left), bright white flares are seen above the level of the fracture surface. Also highlighted are specific GNPs beneath the fracture surface, around which the white flares indicate the presence of voids. This may be compared with the curved GNPs

highlighted in the second image, (right) located 600 μm beneath the fracture surface. It can be seen that there is a clear lack of voids away from the surface, despite the irregular shape of the GNPs that should be an ideal initial location for voids to form. It should be noted that these images are post-mortem and therefore only the largest voids resulting

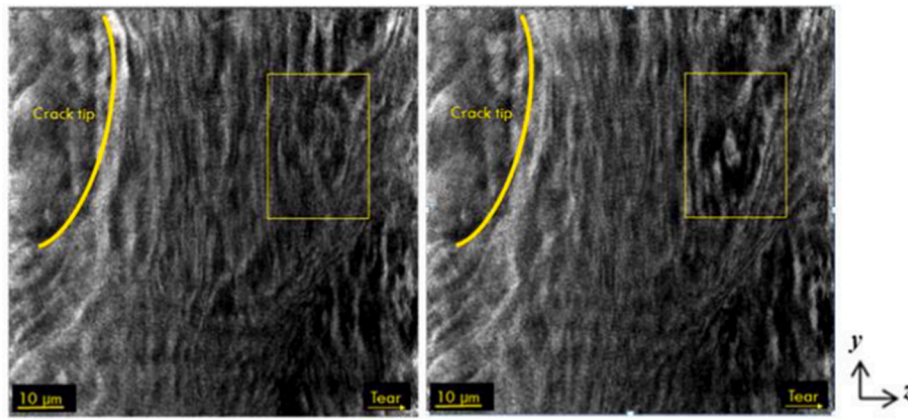


**Fig. 6.** Radiograph showing the tip of a tear propagating across the sample. The direction of the tearing is indicated. A GNP and void formation are seen within the highlighted yellow box. (For interpretation of the references to colour in this figure legend, the reader is referred to the web version of this article.)

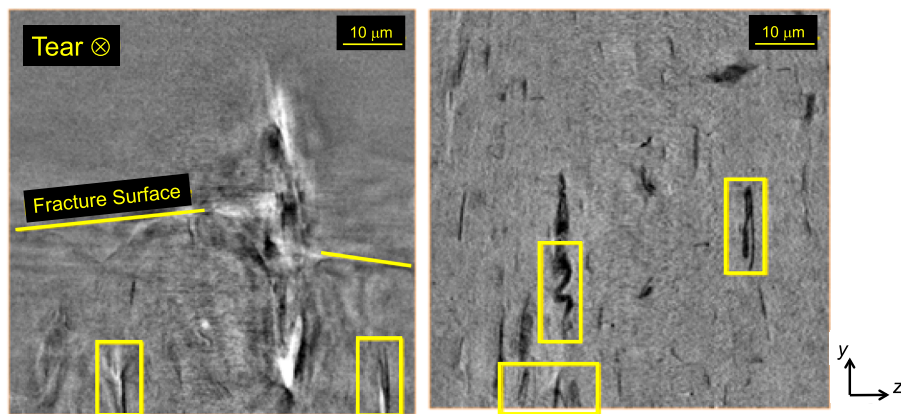


**Fig. 7.** A pair of virtual slices of tomograms taken at (left), and 600  $\mu\text{m}$  beneath (right) the fracture surface respectively. The direction of tear propagation is indicated (left into the page and right in the  $z$  direction). A comparison is made between the two images with respect to the prevalence of voids (white flares in the left image), specifically within the yellow boxes that mark the presence of the GNPs. (For interpretation of the references to colour in this figure legend, the reader is referred to the web version of this article.)

from permanent deformation will be visible on the removal of the load.

The video ([Supplementary Information](#)) and combination of the time-lapse images showing the formation of voids ahead of the crack tip in [Fig. 6](#), together with the cross-sectional images in [Fig. 7](#), show that significant void formation occurs at the tip of the tear during the failure of the NR/GNP nanocomposites. It has also been possible to correlate the X-ray CT scans in [Fig. 7](#) with the local path of tear propagation seen in the SEM micrographs of the fracture surfaces.

### 3.6. Elongation of the voids and specimen failure

As discussed earlier, the formation or nucleation of voids occurs during the deformation of the NR/GNP nanocomposite. Further analysis of the X-ray radiographs yields an insight into the manner by which these voids grow as the tearing takes place. [Fig. 8](#) shows the nanocomposite material just before total rupture and failure and it can be seen that the voids, identified by the dark areas in the image, have become elongated, in contrast with the bright white GNP flakes and grey rubber. In particular, it is seen that the elongation of the voids is uniaxial and along the direction of the applied load ( $y$ ), with the GNPs remaining within the voids.

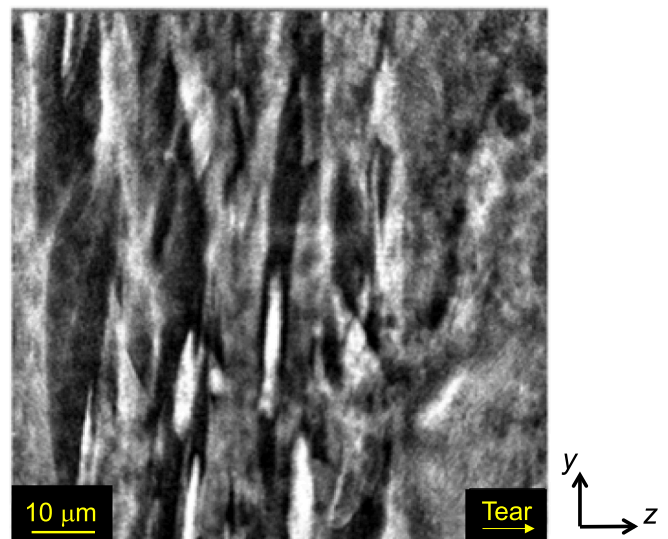


**Fig. 8.** A radiograph showing the elongation of voids around GNPs just ahead of the crack tip before final failure, identified by their bright white appearance and sharp edges. The direction of the tear propagation is  $z$ .

## 4. Analysis of the cavitation and voiding processes

### 4.1. Mechanics of failure

Our earlier study [15] suggested that the increase in fracture energy of a GNP-reinforced elastomers upon the addition of a GNP filler may be the result of a number of different mechanisms: debonding, pull-out and void growth. Hence, we can assume that the overall fracture energy  $G_c$  is given by

$$G_c = G_r + G_{db} + G_{po} + G_v \quad (2)$$

where  $G_r$  is the fracture energy of the pure rubber,  $G_{db}$  is the debonding energy,  $G_{po}$  is the pull-out energy and  $G_v$  is the energy for void formation and growth. A similar relationship was proposed by Chong and co-workers [22] for the fracture energy of GNP-filled epoxy resins, without the term for voiding, which does not occur in their epoxy system.

The current investigation of the failure of these filled elastomers has been undertaken using ASTM tear tests. Although the tear tests are useful for evaluating the relative properties of different rubbers in terms of the tear strength, they do not yield valid fracture mechanics parameters such as strain energy release rate or fracture energy,  $G_c$  [23], because of extensive deformation in the specimen arms. In a recent study [15] we determined the fracture energy for the same FKM/GNP system using the pure shear test that gave valid values of  $G_c$  (in kJ/m<sup>2</sup>). It is interesting to note that the tear strength data in Figs. 2 & 3 are in units of kN/m which is dimensionally equivalent to kJ/m<sup>2</sup>. The tear strength values determined in this present study are compared with the values of fracture energy for the same materials determined in our earlier study [15] in Figure S5 of the Supplementary Information. It can be seen that both sets of data depend linearly upon the volume fraction  $V_f$  of GNPs. Moreover, the tear strength and  $G_c$  both increase by a factor of approximately 3 compared with the pure FKM for a 10 % loading of GNPs. In absolute terms, the value of tear strength is roughly 2x the value of  $G_c$ . Hence it appears that the tear strength from the ASTM tests may be used as a proxy for  $G_c$  to compare the fracture behaviour of the different filled elastomeric materials.

It is clear from Fig. 2 that the addition of GNPs leads to significant similar increases in tearing energy of different elastomers and that the level of toughening is much higher than that obtained for the addition of similar levels of carbon black. Our earlier study [15] showed that the increase in toughness by the addition of GNPs to an FKM/GNP nanocomposite was so high that it could not be explained by debonding and pull-out alone and that other energy absorbing mechanisms such as cavitation and voiding must also be taking place during tear propagation. The direct evidence from the nanoscale X-ray CT analysis presented in our study shows that significant cavitation and void growth occurs during tearing in the GNP filled systems. This can be contrasted with the situation in our carbon black filled elastomers in this present study where we have found a much lower tear energy. Moreover, analysis of the literature [4–7] discussed earlier implies that carbon black does not appear to induce extensive cavitation and voiding during the deformation and tearing of elastomers.

### 4.2. Cavitation and voiding

The X-ray CT scans showed that cavities are nucleated by the breakdown of the interface between the filler particles and the rubber. It is of interest to understand the conditions for the cavities to grow into larger voids, absorbing energy from the creation of new surface and eventually leading to a tear or crack as reviewed by Fond [24]. Gent and co-workers [25–27] have considered the conditions for the expansion of voids within a rubber-like solids, either by internal pressurisation or the application of an external triaxial hydrostatic tensile stress. In their original study, Gent, Lindley and Rideal [25] suggested using the kinetic

theory of rubber elasticity [4] that the relation between inflation pressure  $P$  and the expansion ratio  $\lambda$  of the cavity radius is

$$P/E = (5 - 4\lambda^{-1} - \lambda^{-4})/6 \quad (3)$$

where  $E$  is the small strain Young's modulus of elasticity of the rubber. This equation predicts that a cavity will expand at a critical inflation pressure  $P_c$  of  $5E/6$ . It should be noted that Equation (3) does not contain the cavity radius  $r$  although Gent and co-workers [28,29] subsequently found that small volume voids needed a pressure larger than  $5E/6$  to grow. Gent and Wang [27] suggested that one reason for this size dependence might be the result of surface energy effects because smaller voids with a higher specific surface area might need a higher stress to grow [26]. They proposed that another constraint upon cavitation would be the need for a critical amount of mechanical energy to be released by the propagation of a tear, and that Equation (3) needed to be modified to take this into account.

If it is assumed that a void of initial volume  $V_0$  at the crack tip is inflated by the triaxial hydrostatic stress ahead of the crack to a void of volume  $V$ , then  $V/V_0 = \lambda^3$ . In this case the strain energy  $W$  stored in the rubber is given by

$$W = \int_{V_0}^V P dV \quad (4)$$

Griffith's fracture criterion [23,27] can be invoked to determine the condition for a crack of area  $A$  to grow which is

$$-(\partial W/\partial A)|_V \geq G_r \quad (5)$$

where  $\partial W/\partial A$  is the strain energy release rate and  $G_r$  is the strain energy release rate or fracture energy of the rubber [23]. It can be assumed that the initial void of radius  $r_0$  forms by the debonding of a filler particle before it expands under a pressure  $P$  to a void of volume  $V$ . The initial void volume is thus given by

$$V_0 = 4\pi r_0^3/3 \quad (6)$$

and the area of the equivalent planar circular crack is then given by

$$A = \pi r_0^2 \quad (7)$$

The Griffith fracture criterion in Equation (5) then becomes [27] (see Supplementary Information)

$$\lambda^4 (\partial/\partial \lambda) [\lambda^{-3} \int_1^\lambda (P/E) \lambda^2 d\lambda] \geq G_r / \frac{4r_0 E}{3} \quad (8)$$

Substitution of the expression for  $P/E$  from Equation (3) into the left-hand side of this Equation, and evaluating the integral and differentiating leads to the condition for void growth becoming

$$(1 + \lambda_c^2 - 2\lambda_c^{-1}) \geq 9G_r/4r_0 E \quad (9)$$

where  $\lambda_c$  is now the critical extension ratio needed for a single void of size  $r_0$  to grow. The values of  $\lambda_c$  predicted from Equation (9) are shown in Fig. 9 using values of fracture energy  $G_r$  of 100 J/m<sup>2</sup> and modulus  $E$  of 2 MPa as suggested by Gent and Wang [27]. The ranges of particle sizes for carbon black and GNPs, and hence the sizes of the voids induced by debonding, are indicated on the plot. The highest possible extension ratio for the rubber before it fails,  $\lambda_{max}$ , is shown as a broken line.

It can be seen that the value of  $\lambda_c$  needed to grow voids around carbon black particles is much higher than that for the larger GNPs. This implies that voiding around GNPs is much more likely than around CB particles in carbon black filled rubber which confirms the observations on the lack of voiding in the CB filled rubbers discussed earlier. Gent and Wang [27] pointed out that the analysis described above is rather simplistic in that it assumes that rubbers obey the kinetic theory of rubber elasticity up to high strains which is not the case. They suggested

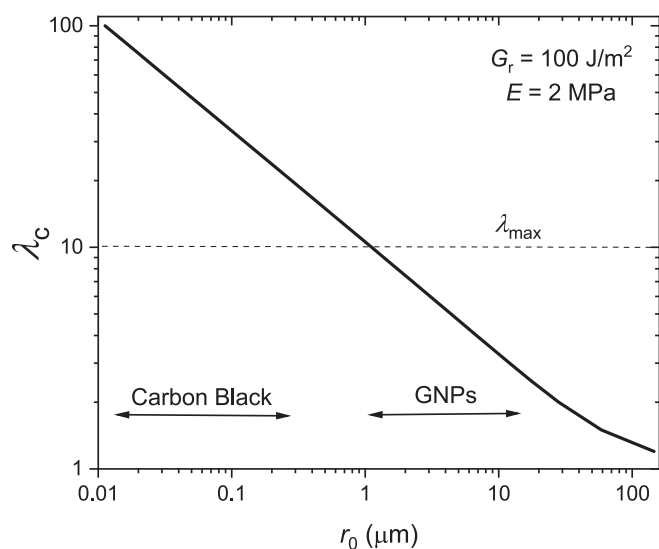


**Fig. 9.** Relationship between the critical extension ratio,  $\lambda_c$  needed to grow void of initial radius,  $r_0$  predicted by Equation (9). The approximate size ranges for carbon black and GNP filler particles (see Fig. 1(b)), that will control the initial void radii, are shown. The maximum possible extension ratio for the rubber before fracture,  $\lambda_{max} = 10$  is indicated [27].

ways in which the theory could be modified to take this into account [27]. Nevertheless such modifications do not change the finding from our simple analysis that voids with a radius smaller than  $\sim 1 \mu\text{m}$  are unlikely to grow under an applied stress. Although our analysis is for a void around a single GNP particle, it is anticipated that it will be valid for higher loadings of multiple particles during tearing.

One issue that has not been considered in this present study is effect of the strength of the interface between the GNP particles and the matrix upon the cavitation and voiding. In an earlier study [30] we found that the addition of silane-functionalised GNPs to a silicone elastomer led to higher levels of stiffness and strength than for the addition of unfunctionalised GNPs. This was shown to be as a result of the stronger interface between the functionalised GNPs and elastomer matrix [30]. It is likely that the findings of this present study would be affected by the strength of the interface between the GNPs and elastomer matrices since the cavities are nucleated by the breakdown of the interface between the filler particles and the rubber. On the other hand we have shown that the growth of the voids is controlled by the fracture energy of the rubber,  $G_r$ , rather than any interfacial parameters. At this stage it is not possible to come to any firm conclusion about the effect of the strength of the interface upon voiding and cavitation and it is clear that interfacial effects should be the subject of future studies upon the mechanisms of toughening of elastomer nanocomposites.

## 5. Conclusions

We have demonstrated that both the tear strength and tearing energy of a number of different types of elastomers can be increased significantly by the addition of graphene nanoplatelets (GNPs) through a combination of mechanisms such as debonding, pull-out and cavitation. This has been contrasted with the addition of carbon black (CB) which had been shown to give significantly lower levels of toughening for the same volume fraction of filler. The processes that occur in the stress field ahead of a tear in natural rubber filled with GNPs have been monitored in situ using nanoscale X-ray computed tomography in a synchrotron. It was found that under stress, the GNP particles debond and form voids that grow which will lead to considerable energy absorption. The mechanisms of cavitation and void growth have been analysed theoretically using the kinetic theory of rubber elasticity and it has been shown that only voids larger than  $1 \mu\text{m}$  in size are likely to grow in the

triaxial tensile stress field ahead of the crack/tear tip. This implies that cavitation and void growth can occur at a lower stress in GNP-filled material with particles  $> 1 \mu\text{m}$  in size than in CB-filled materials with considerably smaller nanofiller particles. Analysis of the previous literature has confirmed our prediction that the amount of cavitation and void growth is limited at the crack/tear tip in CB filled elastomers. The high level of cavitation and void growth found for our GNP-filled elastomers is therefore suggested to be the reason why these nanocomposites have a much higher tear resistance than the CB filled materials. Improved tear resistance in elastomer nanocomposites can lead to the development of longer-lasting and more resilient compounds in sectors such as automotive and aerospace, where durability is paramount. The understanding of the underlying mechanisms and the selection of the most efficient filler materials will have a direct impact on the design and performance of components, ultimately leading to enhanced product quality and reliability.

## CRedit authorship contribution statement

**Conor T. O'Brien:** Data curation, Investigation, Methodology, Writing – original draft. **Zheling Li:** Conceptualization, Methodology. **Mufeng Liu:** Formal analysis, Validation. **J. Robert Innes:** Investigation. **Suhao Li:** Investigation. **Dimitrios G. Papageorgiou:** Conceptualization, Methodology. **Malte Storm:** Investigation, Software. **Timothy L. Burnett:** Conceptualization, Data curation, Funding acquisition, Project administration, Supervision, Writing – review & editing. **Robert J. Young:** Conceptualization, Writing – review & editing.

## Declaration of competing interest

The authors declare the following financial interests/personal relationships which may be considered as potential competing interests: Conor O'Brien reports financial support was provided by The University of Manchester. If there are other authors, they declare that they have no known competing financial interests or personal relationships that could have appeared to influence the work reported in this paper.

## Data availability

Data will be made available on request.

## Acknowledgements

CT O'Brien is grateful to the EPSRC for support from Centre for Doctoral Training in the Science and Applications of Graphene and Related Nanomaterials (GrapheneNOWNANO) (EP/L01548X/1). We are grateful for the provision of beamtime at I13-2, Diamond Light Source under proposal MT20738: 'Understanding the Performance Enhancement in Graphene Reinforced Nanocomposites'. This work was also supported by the National Research Facility for Lab X-ray CT (NXCT) through EPSRC grants EP/T02593X/1 and EP/V035932/1.

## Appendix A. Supplementary data

Supplementary data to this article can be found online at <https://doi.org/10.1016/j.compositesa.2024.108269>.

## References

- [1] Azura AR, Leow SL. Effect of carbon black loading on mechanical, conductivity and ageing properties of Natural Rubber composites. *Mater Today: Proc* 2019;17: 1056–63.
- [2] Li Y, Zhu P, Zhang Q, Chen B, Zhu Z. Study on the properties of rubber with different contents of carbon black. *IOP Conf Ser: Mater Sci Eng* 2019;677(2): 022043.
- [3] Berki P, Göbl R, Karger-Kocsis J. Structure and properties of styrene-butadiene rubber (SBR) with pyrolytic and industrial carbon black. *Polym Test* 2017;61: 404–15.

- [4] Figuera CPM. Relationship Between Structure and Properties in Filled Elastomers [PhD]. Manchester, UK: University of Manchester; 1990.
- [5] Zhang H, Scholz AK, de Crevoisier J, Berghezan D, Narayanan T, Kramer EJ, et al. Nanocavitation around a crack tip in a soft nanocomposite: A scanning microbeam small angle X-ray scattering study. *J Polym Sci B* 2015;53(6):422–9.
- [6] Euchler E, Schneider K, Wiessner S, Bernhardt R, Heinrich G, Roth SV, et al. Cavitation damage in tire rubber materials. In: Huneau B, Cam J-BL, Marco Y, Verron E, editors. *Constitutive Models for Rubber XI*. London: CRC Press; 2019. p. 87–91.
- [7] Xiang F, Schneider K, Schwartzkopf M, Heinrich G. Competition between strain-induced crystallization and cavitation at the crack tip of unfilled and carbon black-filled natural rubber. *Macromolecules* 2022;55(23):10682–93.
- [8] Kallungal J, Chazeau L, Chenal J-M, Adrien J, Maire E, Barrès C, et al. Crack propagation in filled elastomers: 3D study of mechanisms involving the filler agglomerates. *Eng Fract Mech* 2022;274:108771.
- [9] Maire E, Withers PJ. Quantitative X-ray tomography. *Int Mater Rev* 2014;59(1):1–43.
- [10] Li S, Li Z, Burnett TL, Slater TJA, Hashimoto T, Young RJ. Nanocomposites of graphene nanoplatelets in natural rubber: microstructure and mechanisms of reinforcement. *J Mater Sci* 2017;52(16):9558–72.
- [11] Young RJ, Liu M, Kinloch IA, Li S, Zhao X, Vallés C, et al. The mechanics of reinforcement of polymers by graphene nanoplatelets. *Compos Sci Technol* 2018;154:110–6.
- [12] Liu M, Papageorgiou DG, Li S, Lin K, Kinloch IA, Young RJ. Micromechanics of reinforcement of a graphene-based thermoplastic elastomer nanocomposite. *Compos A Appl Sci Manuf* 2018;110:84–92.
- [13] Papageorgiou DG, Kinloch IA, Young RJ. Mechanical properties of graphene and graphene-based nanocomposites. *Prog Mater Sci* 2017;90:75–127.
- [14] Papageorgiou DG, Kinloch IA, Young RJ. Graphene/elastomer nanocomposites. *Carbon* 2015;95:460–84.
- [15] Liu M, Hui JH, Kinloch IA, Young RJ, Papageorgiou DG. Deformation and tearing of graphene-reinforced elastomer nanocomposites. *Compos Commun* 2021;25:100764.
- [16] Hull D, Clyne TW. *An Introduction to Composite Materials*. Cambridge: Cambridge University Press; 1996.
- [17] Liu M, Cataldi P, Young RJ, Papageorgiou DG, Kinloch IA. High-performance fluoroelastomer-graphene nanocomposites for advanced sealing applications. *Compos Sci Technol* 2021;202:108592.
- [18] Kazantsev D, Wadeson N, Basham M. High performance Savu software for fast 3D model-based iterative reconstruction of large data at Diamond Light Source. *SoftwareX* 2022;19:101157.
- [19] Li Z, Deng L, Kinloch IA, Young RJ. Raman spectroscopy of carbon materials and their composites: Graphene, nanotubes and fibres. *Prog Mater Sci* 2023;135:101089.
- [20] Sakulkaew K, Thomas AG, Busfield JJC. The effect of the rate of strain on tearing in rubber. *Polym Test* 2011;30(2):163–72.
- [21] Zernike F. Phase contrast, a new method for the microscopic observation of transparent objects. *Physica* 1942;9(7):686–98.
- [22] Chong HM, Hinder SJ, Taylor AC. Graphene nanoplatelet-modified epoxy: effect of aspect ratio and surface functionality on mechanical properties and toughening mechanisms. *J Mater Sci* 2016;51(19):8764–90.
- [23] Kinloch AJ, Young RJ. *Fracture behaviour of polymers*. Dordrecht: Springer Science & Business Media; 2013.
- [24] Fond C. Cavitation criterion for rubber materials: a review of void-growth models. *J Polym Sci B* 2001;39(17):2081–96.
- [25] Gent AN, Lindley PB, Rideal EK. Internal rupture of bonded rubber cylinders in tension. *Proceedings of the Royal Society of London Series A Mathematical and Physical Sciences*. 1959;249(1257):195–205.
- [26] Gent AN, Tompkins DA. Surface energy effects for small holes or particles in elastomers. *Journal of Polymer Science Part A-2: Polymer Physics* 1969;7(9):1483–7.
- [27] Gent AN, Wang C. Fracture mechanics and cavitation in rubber-like solids. *J Mater Sci* 1991;26(12):3392–5.
- [28] Gent AN, Park B. Failure processes in elastomers at or near a rigid spherical inclusion. *J Mater Sci* 1984;19(6):1947–56.
- [29] Cho K, Gent AN. Cavitation in model elastomeric composites. *J Mater Sci* 1988;23(1):141–4.
- [30] Ren H, Cunha E, Li Z, Wang L, Kinloch IA, Yi D, et al. Silane-functionalized graphene nanoplatelets for silicone rubber nanocomposites. *J Mater Sci* 2022;57(4):2683–96.